Nano Research

Li2SnO3 branched nano- and microstructures with intense and broadband white-light emission
--Manuscript Draft--

Manuscript Number:	NARE-D-18-01505R3
Full Title:	Li2SnO3 branched nano- and microstructures with intense and broadband white-light emission
Article Type:	Regular Article
Corresponding Author:	Miguel García-Tecedor Universitat Jaume I SPAIN
Corresponding Author Secondary Information:	
Corresponding Author's Institution:	Universitat Jaume I
Corresponding Author's Secondary Institution:	
First Author:	Miguel García-Tecedor
First Author Secondary Information:	
Order of Authors:	Miguel García-Tecedor
	Javier Bartolomé
	David Maestre
	Achim Trampert
	Ana Cremades
Order of Authors Secondary Information:	

Abstract:	Exploiting the synergy between microstructure, morphology and dimensions by suitable nanomaterial engineering, can effectively upgrade the physical properties and material performances. Li2SnO3 elongated nano- and microstructures in form of belts, wires, rods and branched structures have been fabricated by a vapor-solid method at temperatures ranging from 700 °C to 900 °C using metallic Sn and Li2CO3 as precursors. The achievement of these new morphologies can face challenging applications for Li2SnO3, not only in the field of energy storage, but also as building blocks in optoelectronic devices. The micro- and nanostructures grown at 700 °C and 800 °C correspond to monoclinic Li2SnO3, while at 900 °C complex Li2SnO3/SnO2 core-shell microstructures are grown, as confirmed by X-ray diffraction and Raman spectroscopy. Transmission electron microscopy reveals structural disorder related to stacking faults in some of the branched structures, which is associated with the presence of the low-temperature phase of Li2SnO3. The luminescent response of these structures is dominated by intense emissions at 2, 2.5 and 3 eV, almost completely covering the whole range of the visible light spectrum. As a result, white-light emission is obtained without the need of phosphors or complex quantum well heterostructures. Enhanced functionality in applications such as in light-emitting devices could be exploited based on the high luminescence intensity observed in some of the analysed Li2SnO3 structures.

Response to Reviewers:	We would like to thank the reviewers for their critical reading, constructive comments and remarks

1
2
3
4
5
6
7
8
9
10
11
12
13
14
15
16
17
18
19
20
21
22
23
24
25
26
27
28
29
30
31
32
33
34
35
36
37
38
39
40
41
42
43
44
45
46
47
48
49
50
51
52
53
54
55
56
57
58
59
60
61
62
63
64
65

Li₂SnO₃ branched nano- and microstructures with intense and broadband white-light emission

M. García-Tecedor,[a*†] J. Bartolomé,[b‡] D. Maestre,[a] A. Trampert,[b] and A. Cremades[a]

([a]) Dpt. Física de Materiales, Facultad de CC. Físicas, Universidad Complutense de Madrid, 28040, Madrid, (Spain).
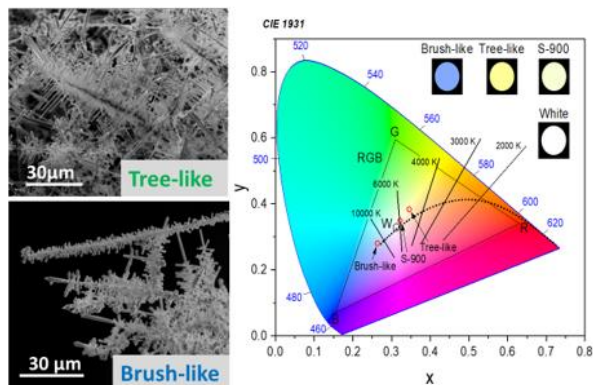
([b]) Paul-Drude-Institut für Festkörperelektronik, Hausvogteiplatz 5−7, 10117 Berlin, Germany.

([*]) **Corresponding author**: M. García-Tecedor
E-mail: tecedor@uji.es   Phone: (+34) 964387555

([†]) Present Address: Institute of Advanced Materials (INAM), Universitat Jaume I, 12006, Castelló, Spain.

([‡]) Present Address: Dpt. Física de Materiales, Facultad de CC. Físicas, Universidad Complutense de Madrid, 28040, Madrid, (Spain)

In the present work, an alternative application of Li₂SnO₃ nano- and microstructures as promising candidates for intense white-light-emitting devices without the use of phosphors or complex quantum structures is proposed for the first time, as far as we know.

M. García-Tecedor (http://www.inam.uji.es/users/miguel-garc%C3%ADa-tecedor)

1
2
3
4
5
6
7
8
9
10
11
12
13
14
15
16
17
18
19
20
21
22
23
24
25
26
27
28
29
30
31
32
33
34
35
36
37
38
39
40
41
42
43
44
45
46
47
48
49
50
51
52
53
54
55
56
57
58
59
60
61
62
63
64
65

Li$_2$SnO$_3$ branched nano- and microstructures with intense and broadband white-light emission

M. García-Tecedor [a†](✉), J. Bartolomé[b‡], D. Maestre[a], A. Trampert[b] and A. Cremades[a]

(*ᵃ*) *Dpt. Física de Materiales, Facultad de CC. Físicas, Universidad Complutense de Madrid, 28040, Madrid, (Spain).*
(*ᵇ*) *Paul-Drude-Institut für Festkörperelektronik, Hausvogteiplatz 5−7, 10117 Berlin, Germany.*
(✉) **Corresponding author**: *M. García-Tecedor*

E-mail: tecedor@uji.es   Phone: (+34) 964387555

(*†*) *Present Address: Institute of Advanced Materials (INAM), Universitat Jaume I, 12006, Castelló, Spain.*

(*‡*) *Present Address: Dpt. Física de Materiales, Facultad de CC. Físicas, Universidad Complutense de Madrid, 28040, Madrid, (Spain)*

ABSTRACT

Exploiting the synergy between microstructure, morphology and dimensions by suitable nanomaterial engineering, can effectively upgrade the physical properties and material performances. Li$_2$SnO$_3$ elongated nano- and microstructures in form of belts, wires, rods and branched structures have been fabricated by a vapor-solid method at temperatures ranging from 700 °C to 900 °C using metallic Sn and Li$_2$CO$_3$ as precursors. The achievement of these new morphologies can face challenging applications for Li$_2$SnO$_3$, not only in the field of energy storage, but also as building blocks in optoelectronic devices. The micro- and nanostructures grown at 700 °C and 800 °C correspond to monoclinic Li$_2$SnO$_3$, while at 900 °C complex Li$_2$SnO$_3$/SnO$_2$ core-shell microstructures are grown, as confirmed by X-ray diffraction and Raman spectroscopy. Transmission electron microscopy reveals structural disorder related to stacking faults in some of the branched structures, which is associated with the presence of the low-temperature phase of Li$_2$SnO$_3$. The luminescent response of these structures is dominated by intense emissions at 2, 2.5 and 3 eV, almost completely covering the whole range of the visible light spectrum. As a result, white-light emission is obtained without the need of phosphors or complex quantum well heterostructures. Enhanced functionality in applications such as in light-emitting devices could be exploited based on the high luminescence intensity observed in some of the analysed Li$_2$SnO$_3$ structures.

Introduction

Among the lithium based oxides, Li_2SnO_3 has aroused increasing attention during the last years due to its applications as dielectric material in the range of microwaves,[1-3] breeding material for nuclear fusion reactors,[4, 5] and mainly in the field of energy storage owing to its use as electrode in Li-ion batteries.[6-8]. There are a relevant number of recent publications combining the use of Li_2SnO_3 with carbon-derived materials, such as graphene, in order to improve the performance of Li ion batteries.[9-11] Besides, Li_2SnO_3 has been reported to exhibit better catalytic properties than other Li ternary oxides, such as Li_2FeO_3 and Li_2ZnO_3.[12] Li_2SnO_3 has been also used as a model in the study of Li diffusion in similar ternary systems. Li_2SnO_3 is usually synthesized in form of bulk material,[2, 12] thin film, or nanoparticles[10, 11] by using different approaches such as the hydrothermal method,[9, 13] sol-gel technique,[14] thermal decomposition,[4] or solid state reactions[15, 16]. There is no published work, as far as we know, related to the fabrication and characterization of elongated nanostructures of Li_2SnO_3, the study of which could broaden the applicability of this material, as they could be used as basic building blocks for electronic and optoelectronic nano- and microdevices. Despite the potential applicability of Li_2SnO_3, many of its fundamental physical properties, such as the bandgap, still remain unclear or under debate. Moreover, the paramount interest recently aroused by the solid-state batteries could hide the applicability of Li_2SnO_3 in alternative fields of research for which this material could also be a promising candidate. Therefore, a better understanding of the synthesis and main properties of Li_2SnO_3 is required to ensure a leap forward in its applicability and performance, not only in the field of Li-ion batteries, but also in other fields of technological relevance, which motivates this study. This work focuses on the growth and characterization of the physical properties of elongated nano- and microstructures of Li_2SnO_3. These nanostructures are found to present a very intense white-light emission, revealing a new potential application of this material. With the replacement of the traditional incandescent light bulbs by the more efficient light emitting devices (LED) for general illumination, finding proper materials capable of emit broadband white light has become the focus of an intense research. Currently white light emission is obtained by either the use of blue/UV LEDs combined with phosphors, which usually have poor colour rendering, or by the fabrication of more complex (In,Ga)N quantum wells, which present a series of problems related to the In incorporation limit, the quantum confined stark effect or the Auger recombination, among others.[17] Thus, the observed capability of the obtained structures of emitting broadband white-light without the need of phosphors or complex quantum well structures is presented as a promising new application of Li_2SnO_3.

Methods

A vapor-solid method, using a controlled mixture of metallic Sn (Aldrich 99.9% purity) and 10 wt.% Li_2CO_3 (Labkem 99.0 %) as precursor, has been employed in this work. The precursor powders were milled in a centrifugal ball mill, in order to homogenize the initial mixture, and then pressed into pellets. Thermal treatments were carried out under argon flow at temperatures of 700, 800 and 900 °C for 5 hours, leading to the growth of nano- and microstructures on the surface of the treated pellets which act simultaneously as source of precursor material, and as substrate for the grown structures. This variation of the vapour-solid (VS) has been successfully used to synthetize nano and microstructures of different semiconducting oxides such as SnO_2, TiO_2 or IZO.[18-21] X-ray diffraction (XRD) measurements were performed in a Philips

X'Pert Pro diffractometer using Cu Kα radiation. The morphological and structural characterization was performed using a Leica 440 Steroscan scanning electron microscope (SEM) and a JEOL JEM 3010 transmission electron microscope (TEM) operated at 300 kV, respectively. Prior to TEM measurements the structures were detached from the pellets, dispersed in isopropanol using an ultrasonic bath and deposited on a Cu mesh grid covered with a C membrane. Compositional analysis was performed by energy dispersive spectroscopy (EDS) in a Leica 440 Stereoscan SEM at 20 kV and 1.5 nA, using a XFlash 4010 detector, whereas the presence of Li was assessed by means of electron energy loss spectroscopy (EELS) on the JEOL JEM 3010 TEM at 300 kV, using a Gatan Enfina spectrometer. Raman characterization was performed at room temperature with a Horiba Jobin-Yvon LabRam Hr800 confocal microscope using a 325 nm He-Cd laser and a 633 nm He-Ne laser. Photoelectron Spectroscopy measurements were performed at Spectromicroscopy beamline, at the Elettra synchrotron facilities, using an incident photon energy of 74 eV. The pellets with the nano- and microstructures were placed on a sample holder and fixed with the help of two Ta strips. The XPS spectra were calibrated with the Ta peak from the strips holders. The spatial and spectral resolution was of ~1 μm and 14 meV respectively. Cathodoluminescence (CL) measurements in the visible range were carried out at 18 kV and at 300 K and 100 K in a Hitachi S2500 SEM using a Hamamatsu PMA-11 CCD. Micro-photoluminescence (μ-PL) was carried out at room temperature using a Horiba Jobin-Yvon LabRam Hr800 confocal microscope and a He-Cd laser (λ=325 nm) as excitation source.

Results and discussion

Following the vapor-solid method, the growth of nanostructures is initiated at 700 °C. Treatments at 800 °C lead to the highest concentration of nano- and microstructures, while treatments carried out at 900 °C resulted in the growth of bigger structures with complex morphologies. The thermal treatments have been repeated several times in order to assure the reproducibility of the results. The samples studied in this work will be named, hereinafter, as S-700, S-800 and S-900, indicating the corresponding growth temperature. XRD measurements have been carried out in normal incidence for the as-grown samples, which present nano- and/or microstructures on the pellet surface. As a result, information from the nano- and microstructures, as well as from the surface of the pellets, is extracted from the XRD signal. Illustratively, the XRD pattern corresponding to the sample S-800, as a representative example, is shown in Figure 1a. The patterns confirm the presence of two different compounds, namely the ternary Li_2SnO_3 compound, with monoclinic crystalline structure (Figure 1b) and lattice parameters of a=5.289 Å, b=9.187 Å and c=10.060 Å,[22] and the rutile tetragonal structure characteristic of SnO_2, with lattice parameters of a=b=4.738 Å, c=3.187 Å.[23] Peaks corresponding to metallic Sn or Li_2CO_3, used as precursors, or to other ternary Li-Sn-O compounds are not observed.
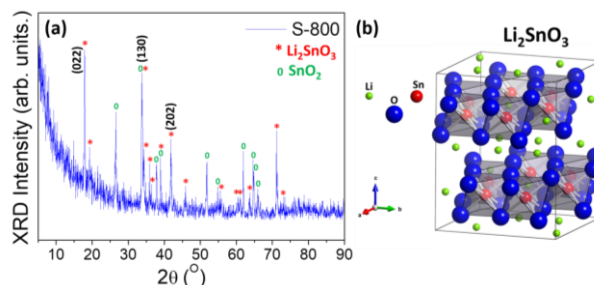
Figure 1. (a) XRD pattern acquired on the sample S-800. (b) Scheme of the monoclinic structure of Li_2SnO_3 obtained with Vesta software.

As previously mentioned, modifications in the morphology and size of the as-grown structures are induced as a function of the different temperatures

used in the thermal treatments. Figure 2 shows SEM images of representative nano- and microstructures corresponding to samples S-700 (a and b), S-800 (c, d, e and f) and S-900 (g and h).
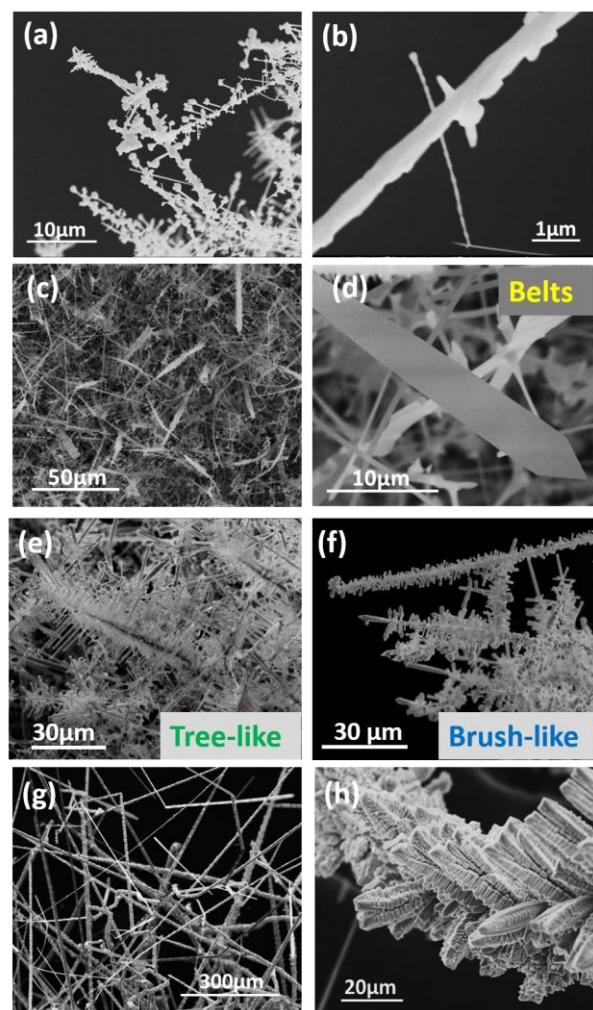
Figure 2. SEM images of nano- and microstructures corresponding to samples S-700 (a, b), S-800 (c, d, e, f) and S-900 (g, h).

A small amount of nanostructures were grown at 700 °C, most of them showing a branched appearance, as observed in Figure 2a. In Figure 2b, initial stages of the formation of the branched nanostructures can be appreciated, where small bumps emerge from the surface of the central branch. These nanostructures present lengths of tens of μm on average, and widths between few μm in the central branch and hundreds of nm in the lateral ones. Increasing the temperature up to 800 °C leads to a notorious increment in the amount of structures, which fully cover the surface of the pellet, as shown in Figures 2c. Moreover, in this case the elongated structures are more developed, with larger sizes and a more defined branched appearance, as compared with those grown at 700 °C. The central branches of these structures usually present thicknesses in the order of μm and lengths of several tens of μm, while the lateral branches, which form angles around 60° with the central stem, exhibit thicknesses ranging from hundreds of nm to a few μm and lengths of several tens of μm. Some of the branched structures are formed by thicker central stems and shorter lateral branches presenting angles of 90° instead, as shown in Figure 2c. In order to distinguish between both structures, they will be hereinafter named as "tree-like" (Figure 2e) and "brush-like" (Figure 2f) structures, respectively. The latter type appears in a lower concentration that the "tree-like" ones. In addition to the branched structures, which appear in a high concentration, nanowires and belts (Figure 2d) with lengths of several tens of μm, widths of few μm and thicknesses of hundreds of nm can be also observed in a lower concentration. The microstructures grown at 900 °C (Figures 2g and 2h) present widths of tens of μm and lengths of hundreds of μm or even mm. Treatments at 900 °C induce an increment in the size of the microstructures which present rod-like shapes with variable growth directions (Figure 2g). Moreover, stepped surfaces and secondary growths are also observed in these microstructures, which results in complex morphologies, as observed in Figure 2h.
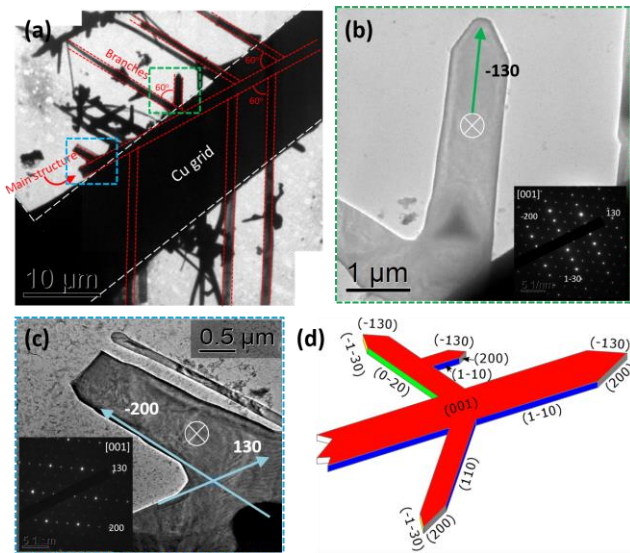
Figure 3. (a) Low magnification TEM image of a tree-like nanostructure grown at 800 °C, showing angles of 60° between the central and lateral branches. (b), (c) Magnified images of the branches marked with dashed squares in (a). The arrows indicate the orientation of the crystallographic planes. Insets show the corresponding SAED patterns acquired along the [001] axis at the marked spots. (d) Scheme of the tree-like structure showing its enclosing facets and their corresponding crystallographic planes.

Some of the tree-like and brush-like structures grown in the sample S-800 have been analyzed by transmission electron microscopy. In Figure 3a, a tree-like branched structure can be observed on top of the Cu grid. The lateral branches form 60° with the central stem. Figures 3b and 3c show TEM images from the lateral branches marked with dotted squares in Figure 3a. These branches exhibit widths of around 1 µm and lower thicknesses as evidenced by their transparency to the electron beam, indicating a belt-like morphology. Selected area electron diffraction (SAED) patterns acquired in the lateral branches, as well as in the central stem, indicate that the tree-like structure corresponds only to monoclinic Li_2SnO_3. Possible domains associated with the presence of SnO_2 or Sn clusters have not been observed. Based on the SAED patterns acquired in the [001] zone axis, it can be concluded that the branches analyzed in

Figures 3b and 3c grow orthogonally to the family planes (-130) and (-200), respectively. A scheme of a tree-like structure indicating the enclosing facets and the corresponding crystallographic planes is shown in Figure 3d.

A TEM image of a brush-like structure is shown in Figure 4a. In this case the lateral branches grow forming angles about 90° with respect to the central stem, which shows a thickness around 200 nm. The lateral branches show lengths about 1 µm and thicknesses lower than 200 nm. In this case, the decreased electron transparency of the lateral branches, as compared with the tree-like structures, evidences their rod-like geometry. SAED patterns acquired in these structures indicate that they also correspond only to monoclinic Li_2SnO_3.
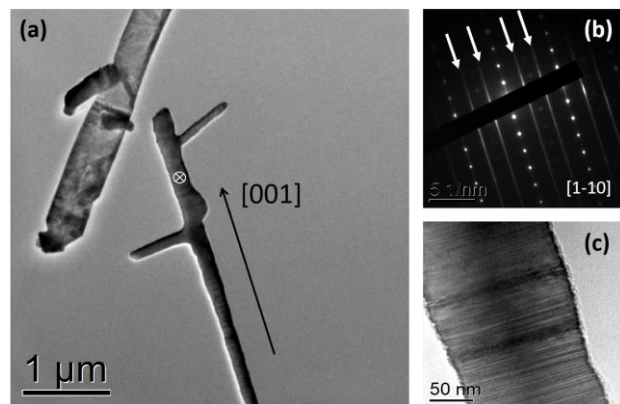
Figure 4. (a) TEM image of a brush-like structure grown in the sample S-800. (b) SAED pattern acquired the region marked with a cross in (a) where diffuse scattering due to stacking disorder can be observed (marked with arrows). (c) Detail of the central stem of the brush-like structure showing stacking faults.

TEM observations reveal that the central stem grows along the [001] direction. Some diffuse streaks can be clearly observed in the [1-10] SAED pattern acquired in the central stem (Figure 4b), which indicates stacking disorder along the c-axis. This disorder can be appreciated in Figure 4c as stripes (stacking faults) perpendicular to the growth axis. The presence of structural disorder associated

with stacking faults along c-axis in Li_2SnO_3 crystals has already been studied by Tarakina et al.[24, 25] In that work the authors reported that Li_2SnO_3 can be synthesized in two phases: the low-temperature (LT)-Li_2SnO_3, formed at temperatures below 800 °C, and the high-temperature (HT)-Li_2SnO_3, which is formed at temperatures above 1000 °C. Both phases are monoclinic, but exhibit slightly different lattice parameters, and correspond to C2/m and C2/c space groups, respectively. In both cases the oxygen atoms form a distorted cubic network with octahedral positions occupied by Li^+ and Sn^{4+} cations. According to Tarakina et al.[25] the LT-Li_2SnO_3 structure would exhibit large amounts of stacking faults along the c-axis. However, the crystalline structure of LT-Li_2SnO_3 is not yet clear and some authors propose that the transition between LT and HT-Li_2SnO_3 consists on the elimination of the defects in the disordered structure through heating treatments.[22] Tarakina et al.[24] compare two Li salts of Li_2MO_3 type (M=Sn, Ti) proposing that the crystal structure of the LT-Li_2MO_3 phase can be described as stacking faults of the LiM_2 (M=Sn, Ti) layers. In our case, the stacking disorder observed in the central stem of the brush-like structures (Figure 4c) could indicate the presence of the LT-Li_2SnO_3 phase at 800 °C. In the case of the tree-like structures, however, we cannot discriminate between the HT and the LT modifications as they always lay on the Cu grid along their c-plane, making the [100] and [110] zone axes inaccessible due to the limited tilting angle of the sample holder.

The TEM study of structures grown at 900 °C is limited by their micrometric size, therefore Raman spectroscopy measurements have been carried out with micrometric resolution in individual micro- and nanostructures in order to analyze their structural characteristics. Raman spectra have been also acquired on samples S-700 and S-800 for comparison. A red-laser (λ=633 nm) and a UV-laser (λ=325 nm) laser have been used during the analysis in a confocal microscope.
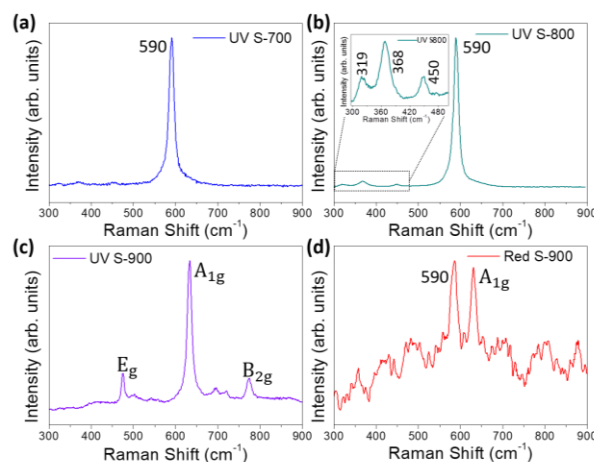

Figure 5. Raman spectra acquired on samples (a) S-700, (b) S-800 and (c, d) S-900. The measurements have been carried out by using an UV laser of 325 nm (He-Cd). In the sample S-900 a red laser of 633 nm (He-Ne) has also been used.

Figure 5a shows the Raman spectrum acquired with the UV-laser on single nanostructures from sample S-700. The corresponding spectrum is dominated by an intense peak at 590 cm^{-1} although some other weak peaks at about 320, 370 and 450 cm^{-1} are also detected. All these peaks correspond to the vibrational modes of Li_2SnO_3.[2] Peaks from SnO_2 or metallic tin are not observed in the Raman spectra, confirming that SnO_2 signal in the XRD patterns come from the pellet (see supporting information S1). Raman spectrum acquired with the UV laser on the nano- and microstructures grown in the sample S-800 is shown in Figure 5b. The spectrum is dominated by the peak at 590 cm^{-1} from monoclinic Li_2SnO_3, as for the S-700 structures. In this case, the spectrum shows higher intensity than for S-700 and the peaks at low energy appear better defined, as shown in the inset in Figure 5b. Three peaks can be observed at 319, 368 and 450 cm^{-1} which correspond to monoclinic Li_2SnO_3, in agreement with TEM observations. In this case, no remarkable differences

have been observed in the Raman spectra corresponding to tree-like or brush-like structures. Moreover, peaks from metallic Sn or SnO_2 have not been detected, which indicates that the peaks from rutile SnO_2 observed in the XRD spectra (Figure 1a) should be related to the presence of tin oxide in the surface of the pellets, but not in the as-grown micro- and nanostructures which only consist of Li_2SnO_3, in agreement with TEM results. Raman spectra have been also acquired on microstructures from sample S-900 using different lasers. Figures 5c and 5d show the Raman spectra acquired by using a UV laser and a red laser, respectively. The penetration depth of the red-laser in Li_2SnO_3 is higher than that of the UV-laser, hence information in depth can be extracted from the Raman analysis using both lasers. The Raman spectrum acquired with the UV-laser in the microstructures from sample S-900 shows only peaks corresponding to rutile SnO_2 (Figure 5c). Three main vibrational modes can be observed at 474 cm^{-1} (E_g), 633 cm^{-1} (A_{1g}) and 778 cm^{-1} (B_{2g}), as usually reported for rutile SnO_2.[26] On the contrary, Raman spectrum acquired with the red-laser (Figure 5d) shows Raman peaks from both Li_2SnO_3 and SnO_2. The coexistence of the vibrational modes of Li_2SnO_3 and SnO_2 at 590 and 633 cm^{-1}, respectively, can be clearly observed in the spectrum. These results suggest that Li_2SnO_3 is present in the inner part of the microstructures grown at 900 °C while the outer part is formed also by SnO_2 and/or Li doped SnO_2.

Compositional analysis has been also performed on the sample S-800, as this sample has been more deeply investigated in this work due to its variable morphology and appropriate dimensions. Compositional analysis by means of EDS was also performed on individual structures from sample S-800 detached from the pellet and placed onto a Cu sample holder. EDS spectra and images (Figure S2) indicate that O and Sn are homogeneously distributed along the structures. As lithium is a

light element it cannot be detected by EDS. In order to confirm the presence of Li in the as-grown structures EELS and XPS measurements have been carried out on the S-800 sample.
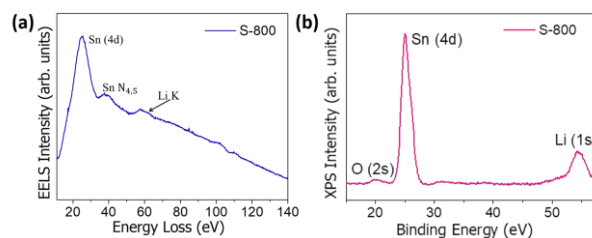

Figure 6. (a) EELS and (b) XPS spectra acquired in structures from sample S-800.

Figure 6a shows the EELS spectrum from sample S-800 formed by the plasmon peak at 25 eV and the Li K-edge at 55 eV.[27] In this case, the Sn $N_{4,5}$-edge at 24 eV is overshadowed by the plasmon peak. EELS spectra acquired in different micro- and nanostructures confirm the incorporation of Li into the structures, however their large thickness reduces the signal-to-background ratio of the EELS edges, hindering the proper quantification. Complementary XPS measurements were performed to further assess the incorporation of Li in the structures. The photoemission spectrum in Figure 6b shows peaks at 20 eV, 25 eV and 54 eV corresponding to the O (2s), Sn (4d) and Li (1s) core levels, respectively [28,29], confirming the incorporation of Li in the structures. Photoelectron spectroscopy is a surface-sensitive technique and the relationship between Li and Sn content at the surface of the probed structures could be estimated for the division of the areas of the peaks related to each element, extracted from the experimental photoemission spectra, and corrected with the effective cross section of each element at the excitation energy of the beam (74 eV in our case). In this case, the estimated Li/Sn ratio at the surface of the structures is around 4.4, which is higher than the stoichiometric one for Li_2SnO_3, which is 2. This

obtained value points out that the Li concentration is higher at the surface, possibly due to some diffusion of the Li atoms to the surface. Recent theoretical calculations demonstrate that surfaces with a low amount of Li in excess are energetically favorable, [30] which agrees with our photoemission spectroscopy results.

The CL response of the samples containing micro and nanostructures was analyzed at room temperature (300 K) and low temperature (100 K), as it can be observed in Figures 7a and 7b, respectively. Figure 7a shows normalized CL spectra from samples S-700, S-800 and S-900 acquired at 300 K and variations can be clearly appreciated as a function of the growth temperature. Remarkably, at room temperature the S-900 sample is the one presenting higher CL intensity, around 50 times higher than the S-700 and 70 times higher than the S-800, which is the sample with less intensity. Moreover, at low temperature the total CL intensity from sample S-900 is 50 times higher than samples S-700 and S-800 which exhibit similar intensity level at 100K. All the spectra are dominated by three main emissions centered at around 2.0, 2.5 and 3.4 eV, however the relative intensity of each one varies as a function of the analyzed sample.
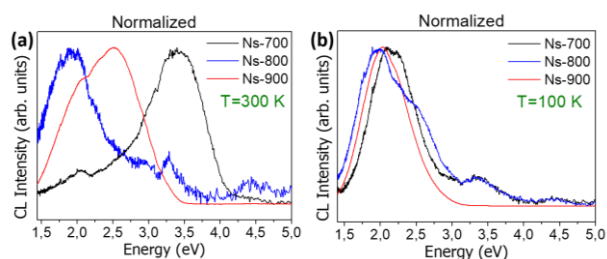
Figure 7. Normalized CL spectra of the structures grown on the samples S-700, S-800 and S-900 acquired at (a) 300 K, and (b) 100 K.

In the sample S-700 the emission centered in 3.4 eV predominates, although small contributions at 2.5 eV and 2.0 eV can be also appreciated. On the other hand, in the spectrum of the sample S-800 the emission centered around 2.0 eV clearly dominates, and the emission at 3.4 eV is also appreciated but with lower relative intensity. In this case, the emission at around 2.5 eV shows a low relative intensity, and a weak emission can be also observed at about 4.4 eV. In the sample S-900 the emission at 2.5 eV dominates the spectrum and the emission at 2.0 eV also exhibits high relative intensity. Figure 7b shows the normalized CL spectra acquired at 100 K in the samples S-700, S-800 and S-900. In this case, the spectra from all the samples show high intensity and all of them are dominated by the emission at about 2.0 eV. Weak shoulders can be appreciated at energies lower and higher than 2 eV, which indicates that this is a complex band formed by different emissions. In this case, emissions at 2.5 and 3.4 eV are nearly quenched at 100 K, indicative of thermally activated processes. This behavior is characteristic of trap-assisted luminescence mechanisms,[31, 32] which could be associated with these emissions. Despite the fact that all the samples exhibit a high CL signal, the intensity of the emission from sample S-900 is much higher than the others, as observed at 300 K. In the samples S-700 and S-800, in addition to the dominant emission at 2.0 eV, other low intensity emissions at higher energies (3.4 and 4.4 eV) can be also appreciated. Deconvolution of the CL spectrum from sample S-800 is included as supplementary information (Figure S3). Works on the luminescence of Li_2SnO_3 are scarce in the scientific literature, therefore the origin of these emissions remain unclear and the results here-shown will help to shed light to their study. Cao et al.[33] studied the luminescence of Li_2SnO_3:Mn^{4+}. In their work, the authors attribute the whole luminescent response of the material to the intraionic transitions of Mn^{4+} ion, rejecting any contribution from the Li_2SnO_3 host, contrary to the notable luminescence response observed in our case for the analyzed micro- and nanostructures. Moritani et al.[5] reported the luminescence of

Li_2SnO_3 under irradiation with H^+ and He^+ ions, which consists of a broad emission between 2 and 4 eV. In that work, the authors reported that this broad emission is formed by bands at 2.3, 2.6, 3.0 and 3.3 eV, although their origin is not clarified. These emissions are similar to some of those observed in our CL spectra. According to our results, the emission centered at 3.4 eV should be associated with the defects involved in the first stages of growth of the nanostructures, as this emission dominates CL spectra from the sample S-700 and reduces its relative intensity as the growth temperature increases. The emission around 2.0 eV is dominant in the sample S-800, where a high amount of Li_2SnO_3 micro- and nanostructures are grown and TEM results indicate the presence of LT-Li_2SnO_3 phase associated with structural disorder along the c-axis. This emission also exhibits high relative intensity for S-900. On the other hand, for the sample S-900 contributions from emissions related to SnO_2 and/or Li doped SnO_2 should be also considered, as Raman spectra indicate the presence of SnO_2 in the outer part of the microstructures. Bands at 1.94 eV, 2.25 eV and 2.58 eV have been reported for SnO_2, being the two first associated with oxygen-vacancies defects and the latter with surface defects in SnO_2.[34] Some of these emissions could overlap the luminescence from Li_2SnO_3. Intraionic transitions $^2P_0$-^2S attributed to Li^+ cations [35] are not observed in this case.

Analogous luminescent behaviors are obtained by photoluminescence acquired at room temperature, showing similar emissions as those already described for CL. PL spectra have been acquired in a confocal microscope, which allows to analyze isolated structures detached from the pellets with micrometric resolution. Figure 8 shows normalized PL spectra acquired, at 300 K using a UV laser (λ = 325 nm) as excitation source, in one tree-like and one brush-like structure from sample S-800. According to TEM and Raman results, these

structures only consist of Li_2SnO_3, with no contribution from SnO_2.
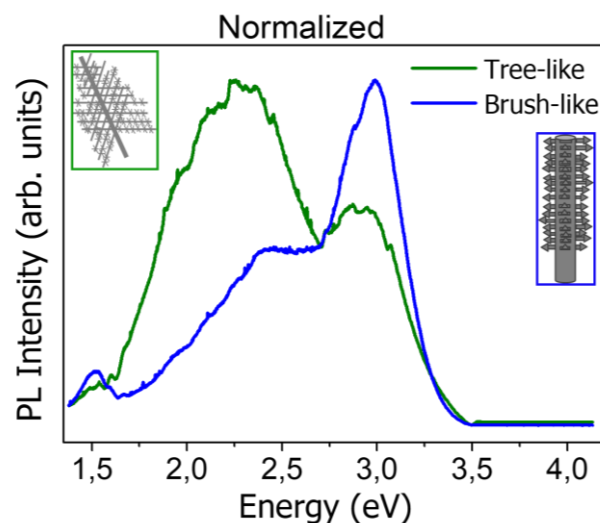
Figure 8. Normalized PL spectra acquired in tree-like (green line) and brush-like (blue line) structures grown at 800 °C. Left and right insets show schemes of the tree-like and brush-like structures, respectively.

The PL signal of the Li_2SnO_3 is characterized by a broad and complex emission in the visible range, with main contributions centered at about 2.1, 2.4 and 3.0 eV. The relative intensity of these emissions varies as a function of the probed structure. The emission at 2.4 eV predominates in the tree-like structures, while in the brush-like structures the emission at 3.0 eV is the dominant one. Deconvolution of the spectra is included in Figures S4b and S4c, as supporting information. Further experiments are required in order to confirm if these emissions are complex and more bands should be included in the deconvolution. Contrary to these PL spectra, no remarkable differences were observed in the Raman spectra corresponding to these tree-like and brush-like structures. Extended defects involved in the growth of each structure, as the presence of stacking faults observed by TEM in the brush-like structures, could be involved in the variations in the relative intensities of these bands.

Li⁺ has several allowed intra-ionic emissions, as reported by different authors. Specifically, it presents an intraionic emission between the ^2S-$^2P_0$ levels centered at 713.5 nm (1.74 eV).[35] In other systems, such as Li doped TiO_2, this emission has been observed slightly shifted at 724 nm.[36] In Li doped Ga_2O_3, I. López et al.[37] observed the presence of a narrow and intense emission around 717 nm (1.73 eV), which was associated with the intra-ionic emission of Li⁺ ions between the ^2S-$^2P_0$ levels again. Even when this energy could be shifted from one matrix to another,[38] in our case a possible relation of the weak emission at 1.5 eV observed in the PL spectrum in Figure 8 with the intra-ionic transitions of Li⁺ ion could be discarded. Actually, this weak emission could be caused by the second-order diffraction peak of the emission at 3.0 eV observed in Figure 8.
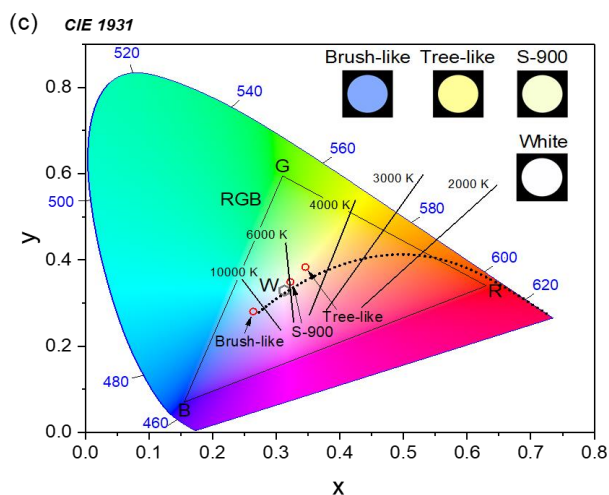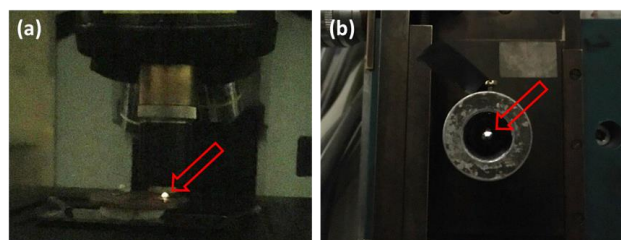
Figure 9. Optical images of (a) PL and (b) CL set-ups where a high luminescent response from sample S-900 (marked with an arrow) can be observed. (c) CIE 1931 chromaticity coordinates

of sample S-900 as well as the tree-like and brush-like structures. The black triangle represents the RGB gamut with the pure red, green and blue coordinates placed in the vertices, and the pure white marked by the gray hexagon. The black dotted line across indicates the color of the black body radiation as a function of the temperature while the solid straight lines mark the color isotherms for particular temperatures. The insets show an enlargement of the color corresponding to each of the chromaticity coordinates calculated for each structure. The pure white color is also shown for comparison.

Although the origin of the defect-related emissions in Li_2SnO_3 cannot be unraveled yet, the luminescence characterization carried out in this work could help to shed light to the discrepancies on the calculated value of the Li_2SnO_3 bandgap. Shein et al.[39] performed theoretical simulations on the electronic properties of some compounds of the Li_2MO_3 family, with M=Ti, Zr and Sn. According to their simulations, the three compounds have a similar band structure with the following bandgaps: 3.5 eV (Li_2TiO_3), 2.9 eV (Li_2ZrO_3) and 1.9 eV (Li_2SnO_3). Stahiya et al.[40] reported bandgap values about 3.0 eV and Howard et al.[30] calculate a wider bandgap of 4 eV for Li_2SnO_3. Despite PL is not the proper method to determine the bandgap of any material, it can still provide a lower estimation of its value as light emission above the bandgap energy would not, in general be expected. Thus, according to our results, Li_2SnO_3 should be a wide-bandgap material, with a minimum E_g value of at least 3.4 eV, in agreement with Howard et al., or even higher considering some of the high-energy emissions observed in the CL spectra. Variations of the E_g as a function of the Li_2SnO_3 phase, LT or HT, should be also considered, as occurring for other wide bandgap semiconductors such as TiO_2, which presents different band gaps for the anatase and rutile phases.[41]

It should be also noticed that CL and PL measurements confirm high luminescence from the samples under study, even at room temperature. Among the analyzed samples, S-900 shows a remarkable high luminescence, so that a bright and intense spot can be observed during the luminescence measurements, as shown in Figure 9a and 9b. This spot presents a white color for which the broad luminescence spectra, ranging from the near infrared to the ultraviolet, is responsible. Considering the wide interest for novel white-light emitting materials we have performed further analysis of the color emission of this sample and compared it with the brush-like and tree-like structures obtained in sample S-800. To this end we have calculated the chromaticity coordinates from their measured spectra following the Commission Internationale de l'Eclairage (CIE) standard. The results are plotted in the chromaticity diagram shown in Figure 9c. As it can been observed, the color emission of sample S-900 (chromaticity coordinates x = 0.322, y = 0.349) lies very close to the pure white (chromaticity coordinates x = 0.313, y = 0.329, as defined by the standard illuminant D65). In comparison the tree-like and brush-like structures present a yellower and bluer color respectively, with chromaticity coordinates of (0.346, 0.384) and (0.264, 0.280). The correlated color temperature (CCT) of sample S-900 is 5944 K, relatively close to the D65 standard (CCT = 6504 K) while the tree-like structure presents a CCT of 5071 K, very close to the value of a typical fluorescent light source (~5000 K).

The two traditional approaches to obtain white light from a light emitting diode (LED) are combining LEDs from the three primary colors (red, green and blue) [42] or the use of a phosphor material, which in combination with a blue or UV-LED usually of GaN or InGaN, broaden the final emission [43, 44]. However, the use of phosphors introduces some disadvantages including short lifetimes and lower efficiencies. In order to avoid these problems, quantum well (QWs) structures were employed for obtaining white light [45, 46]. In the present work, we have shown micro and nanostructures with an intense white light emission without the use of any phosphors or complex structures such as multi quantum wells. This high white luminescence can broaden the applicability of Li_2SnO_3 in the field of phosphor-free light-emitting devices in addition to the well-known lithium-related energy storage applications, while the study of the Li_2SnO_3 physical properties here-shown could improve the general understanding of the material.

Conclusions

In this work different Li_2SnO_3 nano- and microstructures have been fabricated by a vapor-solid method using Sn and Li_2CO_3 as precursors and one-step thermal treatments at 700, 800 and 900 °C for 5h in the presence of an Ar flow. Novel morphologies have been achieved for Li_2SnO_3, leading to potential extended applicability of this material usually employed in the field of energy storage so far. Mainly Li_2SnO_3 branched structures have been obtained at 700 and 800 °C, as confirmed by Raman spectroscopy and SAED measurements performed on individual nanostructures, while at 900 °C complex SnO_2/Li_2SnO_3 core-shell elongated microstructures were fabricated, as revealed by Raman spectroscopy using different excitation wavelengths. Among the branched wires, tree-like and brush-like structures are commonly observed at 800 °C. Structural disorder was detected in the rods grown at 800 °C along the [001] direction, the presence of which could be associated with the low-temperature phase of Li_2SnO_3. In terms of EELS and photoelectron spectroscopy the presence of Li was detected in the structures, with a low amount of Li in excess detected at the surface of the probed

structures. The luminescence response of the nano- and microstructures was studied by CL and PL, showing a complex broad emission formed by several bands in the visible range peaked at about 2.0, 2.5, 3.0 and 3.4 eV. This luminescent study could shed light to the estimation of the E_g value for Li_2SnO_3, which should be about 3.4 eV or even higher. The extremely high white luminescent emission observed in some samples could enhance their functionality in phosphor-free white light-emitting devices.

Acknowledgements

Electronic Supplementary Material: Supplementary material (EDS analysis, and the deconvolutions of the CL and PL spectra are shown in the Electronic Supplementary Information.) is available in the online version of this article at http://dx.doi.org/10.1007/s12274-***-****-* (automatically inserted by the publisher).

References

[1]   Pang, L. X.; Zhou, D. Microwave dielectric properties of low- firing Li_2MO_3 (M= Ti, Zr, Sn) ceramics with B_2O_3–CuO addition. *Journal of the American Ceramic Society* **2010**, *93*, 3614-3617.

[2]   Fu, Z.;Liu, P.;Ma, J.;Guo, B.;Chen, X.; Zhang, H. Microwave dielectric properties of low-fired Li_2SnO_3 ceramics co-doped with MgO–LiF. *Materials Research Bulletin* **2016**, *77*, 78-83.

[3]   Liu, C.;Wu, N.;Mao, Y.; Bian, J. Phase formation, microstructure and microwave dielectric properties of Li_2SnO_3-MO (M= Mg, Zn,) ceramics. *Journal of Electroceramics* **2014**, *32*, 199-204.

[4]   Inagaki, M.;Nakai, S.; Ikeda, T. Synthesis and sintering of Li_2SnO_3. *Journal of Nuclear Materials* **1988**, *160*, 224-228.

[5]   Moritani, K.; Moriyama, H. In situ luminescence measurement of irradiation defects in ternary lithium ceramics under ion beam irradiation. *Journal of nuclear materials* **1997**, *248*, 132-139.

[6]   Idota, Y.;Kubota, T.;Matsufuji, A.;Maekawa, Y.; Miyasaka, T. Tin-based amorphous oxide: a high-capacity lithium-ion-storage material. *Science* **1997**, *276*, 1395-1397.

[7]   Courtney, I. A.; Dahn, J. Electrochemical and in situ X- ray diffraction studies of the reaction of lithium with tin oxide composites. *Journal of the Electrochemical Society* **1997**, *144*, 2045-2052.

[8]   Fang, L.; Chowdari, B. Sn–Ca amorphous alloy as anode for lithium ion battery. *Journal of power sources* **2001**, *97*, 181-184.

[9]   Wang, Q.;Huang, Y.;Miao, J.;Wang, Y.; Zhao, Y. Hydrothermal derived Li_2SnO_3/C composite as negative electrode materials for lithium-ion batteries. *Applied Surface Science* **2012**, *258*, 6923-6929.

[10]   Zhao, Y.;Huang, Y.;Wang, Q.;Wang, X.; Zong, M. Carbon-doped Li_2SnO_3/graphene as an anode material for lithium-ion batteries. *Ceramics International* **2013**, *39*, 1741-1747.

[11]   Zhao, Y.;Huang, Y.;Wang, Q.;Wang, X.;Zong, M.;Wu, H.; Zhang, W. Graphene supported Li_2SnO_3 as anode material for lithium-ion batteries. *Electronic Materials Letters* **2013**, *9*, 683-686.

[12]   Huang, Y.;Wang, G.;Wu, T.; Peng, S. Catalytic oxydehydrogenation of isobutane over lithium-based oxides. *Journal of Natural Gas Quemistry* **1998**, *7*, 102-107.

[13]   Zhao, Y.;Huang, Y.; Wang, Q. Graphene supported poly-pyrrole (PPY)/ Li_2SnO_3 ternary composites as

anode materials for lithium ion batteries. *Ceramics International* **2013**, *39*, 6861-6866.

[14] Zhang, D.;Zhang, S.;Jin, Y.;Yi, T.;Xie, S.; Chen, C. Li_2SnO_3 derived secondary Li–Sn alloy electrode for lithium-ion batteries. *Journal of alloys and compounds* **2006**, *415*, 229-233.

[15] Belliard, F.; Irvine, J. Electrochemical comparison between SnO_2 and Li_2SnO_3 synthesized at high and low temperatures. *Ionics* **2001**, *7*, 16-21.

[16] Zhao, Y.;Li, X.;Yan, B.;Xiong, D.;Li, D.;Lawes, S.; Sun, X. Recent Developments and Understanding of Novel Mixed Transition- Metal Oxides as Anodes in Lithium Ion Batteries. *Advanced Energy Materials* **2016**, *6*.

[17] O'donnell, K.;Auf der Maur, M.;Di Carlo, A.; Lorenz, K. It's not easy being green: Strategies for all- nitrides, all- colour solid state lighting. *physica status solidi (RRL)–Rapid Research Letters* **2012**, *6*, 49-52.

[18] García-Tecedor, M.;Maestre, D.;Cremades, A.; Piqueras, J. Growth and characterization of Cr doped SnO_2 microtubes with resonant cavity modes. *Journal of Materials Chemistry C* **2016**, *4*, 5709-5716.

[19] García-Tecedor, M.;Maestre, D.;Cremades, A.; Piqueras, J. Tailoring optical resonant cavity modes in SnO_2 microstructures through doping and shape engineering. *Journal of Physics D: Applied Physics* **2017**, *50*, 415104.

[20] Vásquez, G. C.;Peche-Herrero, M. A.;Maestre, D.;Cremades, A.;Ramírez-Castellanos, J.;González-Calbet, J. M.; Piqueras, J. Cr doped titania microtubes and microrods synthesized by a vapor–solid method. *CrystEngComm* **2013**, *15*, 5490-5495.

[21] Bartolomé, J.;Maestre, D.;Amati, M.;Cremades, A.; Piqueras, J. Indium zinc oxide pyramids with pinholes and nanopipes. *The Journal of Physical Chemistry C* **2011**, *115*, 8354-8360.

[22] Hodeau, J.;Marezio, M.;Santoro, A.; Roth, R. Neutron profile refinement of the structures of Li_2SnO_3 and Li_2ZrO_3. *Journal of Solid State Chemistry* **1982**, *45*, 170-179.

[23] Bolzan, A. A.;Fong, C.;Kennedy, B. J.; Howard, C. J. Structural studies of rutile-type metal dioxides. *Acta Crystallographica Section B: Structural Science* **1997**, *53*, 373-380.

[24] Tarakina, N. V.;Denisova, T. A.;Baklanova, Y. V.;Maksimova, L. G.;Zubkov, V. G.; Neder, R. B. Defect Crystal Structure of Low Temperature Modifications of Li_2MO_3 (M= Ti, Sn) and Related Hydroxides. In *Advances in Science and Technology*; Trans Tech Publ, 2010; pp 352-357.

[25] Tarakina, N. V.;Denisova, T.;Maksimova, L.;Baklanova, Y.;Tyutyunnik, A.;Berger, I.;Zubkov, V.; Van Tendeloo, G. Investigation of stacking disorder in Li_2SnO_3. *Z. Kristall* **2009**, *36*, 37.

[26] Livneh, T.;Lilach, Y.;Popov, I.;Kolmakov, A.; Moskovits, M. Polarized raman scattering from a single, segmented SnO_2 wire. *The Journal of Physical Chemistry C* **2011**, *115*, 17270-17277.

[27] http://www.eels.info/atlas.

[28] Wang, Q.;Huang, Y.;Miao, J.;Zhao, Y.; Wang, Y. Synthesis and properties of carbon-doped Li_2SnO_3 nanocomposite as cathode material for lithium-ion batteries. *Materials Letters* **2012**, *71*, 66-69.

[29] Charles, D.;Naumkin, A. V.; Kraut-Vass, A. W. NIST X-ray photoelectron spectroscopy database. **2005**.

[30] Howard, J.; Holzwarth, N. First-principles simulations of the porous layered calcogenides $Li_{2+x}SnO_3$ and $Li_{2+x}SnS_3$. *Physical Review B* **2016**, *94*, 064108.

[31] Valerini, D.;Creti, A.;Lomascolo, M.;Manna, L.;Cingolani, R.; Anni, M. Temperature dependence of the photoluminescence properties of colloidal CdSe∕ZnS core/shell quantum dots embedded in a polystyrene matrix. Physical Review B 2005, 71, 235409.

[32] Gaponenko, M. S.;Lutich, A. A.;Tolstik, N. A.;Onushchenko, A. A.;Malyarevich, A. M.;Petrov, E. P.; Yumashev, K. V. Temperature-dependent photoluminescence of PbS quantum dots in glass: Evidence of exciton state splitting and carrier trapping. Physical Review B 2010, 82, 125320.

[33] Cao, R.;Wang, W.;Zhang, J.;Jiang, S.;Chen, Z.;Li, W.; Yu, X. Synthesis and luminescence properties of Li_2SnO_3: Mn^{4+} red-emitting phosphor for solid-state lighting. *Journal of Alloys and Compounds* **2017**, *704*, 124-130.

[34] Maestre, D.;Cremades, A.; Piqueras, J. Growth and luminescence properties of micro-and nanotubes in sintered tin oxide. *Journal of applied physics* **2005**, *97*, 044316.

[35] Wiese, W.; Fuhr, J. Accurate atomic transition probabilities for hydrogen, helium, and lithium. *Journal of physical and chemical reference data* **2009**, *38*, 565-720.

[36] Kallel, W.;Bouattour, S.;Ferreira, L. V.; do Rego, A. B. Synthesis, XPS and luminescence (investigations) of Li^+ and/or Y^{3+} doped nanosized titanium oxide. *Materials Chemistry and Physics* **2009**, *114*, 304-308.

[37] López, I.;Alonso-Orts, M.;Nogales, E.;Méndez, B.; Piqueras, J. Influence of Li doping on the morphology and luminescence of Ga_2O_3 microrods grown by a vapor-solid method. *Semiconductor Science and Technology* **2016**, *31*, 115003.

[38] Imbusch, G.; Henderson, B. Optical spectroscopy of inorganic solids. Clarendon Press, Oxford, 1989.

[39] Shein, I.;Denisova, T.;Baklanova, Y. V.; Ivanovskii, A. Structural, electronic properties and chemical bonding in protonated lithium metallates $Li_{2-x}H_xMO_3$ (M= Ti, Zr, Sn). *Journal of Structural Chemistry* **2011**, *52*, 1043-1050.

[40] Sathiya, M.;Rousse, G.;Ramesha, K.;Laisa, C.;Vezin, H.;Sougrati, M. T.;Doublet, M.-L.;Foix, D.;Gonbeau, D.; Walker, W. Reversible anionic redox chemistry in high-capacity layered-oxide electrodes. *Nature materials* **2013**, *12*, 827.

[41] Di Valentin, C.;Pacchioni, G.; Selloni, A. Origin of the different photoactivity of N-doped anatase and rutile TiO_2. *Physical Review B* **2004**, *70*, 085116.

[42] Muthu, S.;Schuurmans, F. J.; Pashley, M. D. Red, green, and blue LEDs for white light illumination. *IEEE Journal of selected topics in quantum electronics* **2002**, *8*, 333-338.

[43] Park, J. K.;Lim, M. A.;Kim, C. H.;Park, H. D.;Park, J. T.; Choi, S. Y. White light-emitting diodes of GaN-based Sr_2SiO_4: Eu and the luminescent properties. *Applied Physics Letters* **2003**, *82*, 683-685.

[44] Kim, J. S.;Jeon, P. E.;Park, Y. H.;Choi, J. C.;Park, H. L.;Kim, G. C.; Kim, T. W. White-light generation through ultraviolet-emitting diode and white-emitting phosphor. *Applied Physics Letters* **2004**, *85*, 3696-3698.

[45] Yamada, M.;Narukawa, Y.; Mukai, T. Phosphor free high-luminous-efficiency white light-emitting diodes compo sed of InGaN multi-quantum well. *Japanese Journal of Applied Physics* **2002**, *41*, L246.

[46] Huang, C.-F.;Lu, C.-F.;Tang, T.-Y.;Huang, J.-J.; Yang, C. Phosphor-free white-light light-emitting diode of weakly carrier-density-dependent spectrum with prestrained growth of InGaN∕GaN quantum wells. *Applied physics letters* **2007**, *90*, 151122.

Electronic Supplementary Material

Li$_2$SnO$_3$ branched nano- and microstructures with intense and broadband white-light emission

M. García-Tecedor [a†]($\boxtimes$), J. Bartolomé[b‡], D. Maestre[a], A. Trampert[b] and A. Cremades[a]

(*ª*) *Dpt. Física de Materiales, Facultad de CC. Físicas, Universidad Complutense de Madrid, 28040, Madrid, (Spain).*
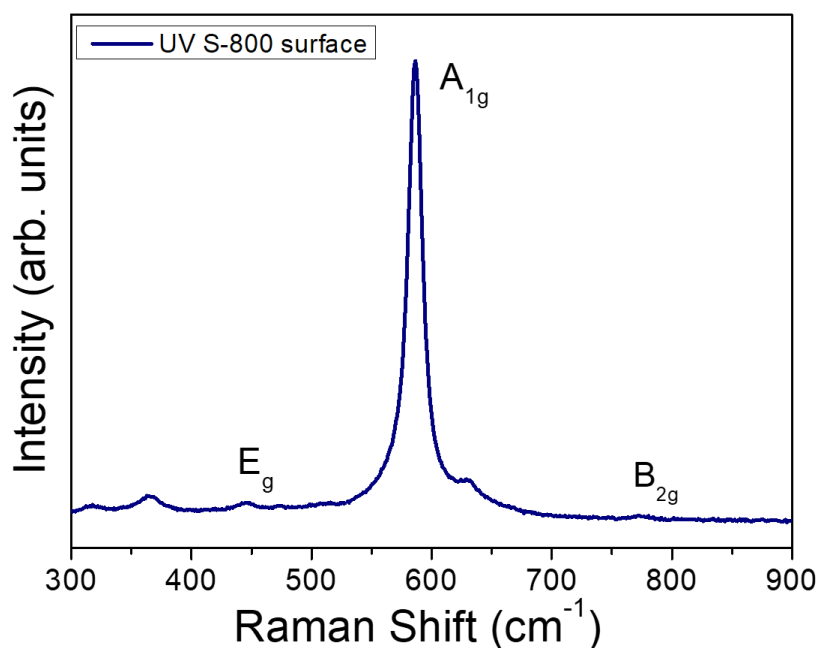(*ᵇ*) *Paul-Drude-Institut für Festkörperelektronik, Hausvogteiplatz 5−7, 10117 Berlin, Germany.*
($\boxtimes$) ***Corresponding author****: M. García-Tecedor*

E-mail: tecedor@uji.es   *Phone: (+34) 964387555*
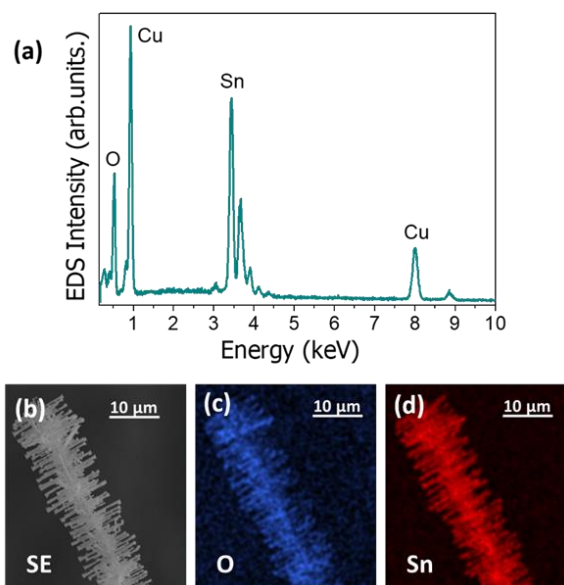
(*†*) *Present Address: Institute of Advanced Materials (INAM), Universitat Jaume I, 12006, Castelló, Spain.*

(*‡*) *Present Address: Dpt. Física de Materiales, Facultad de CC. Físicas, Universidad Complutense de Madrid, 28040, Madrid, (Spain)*
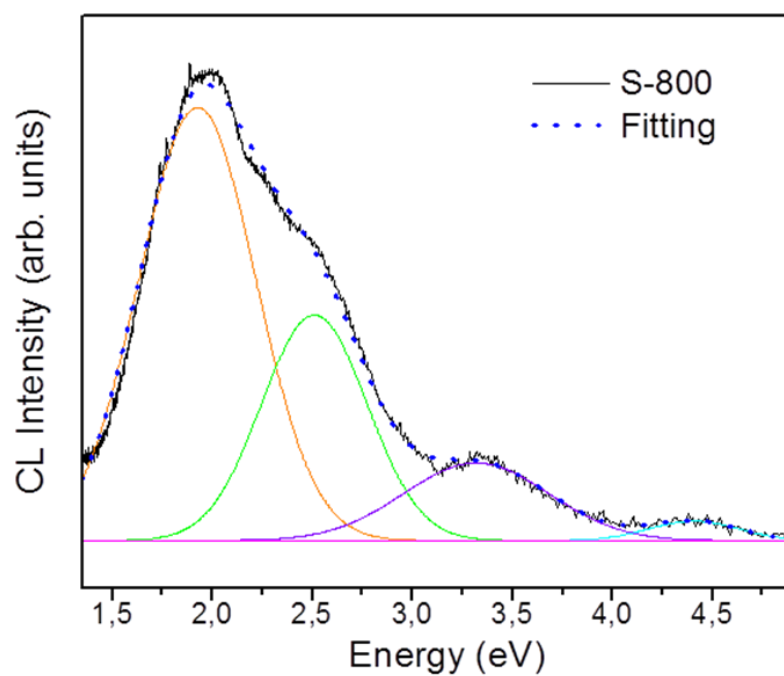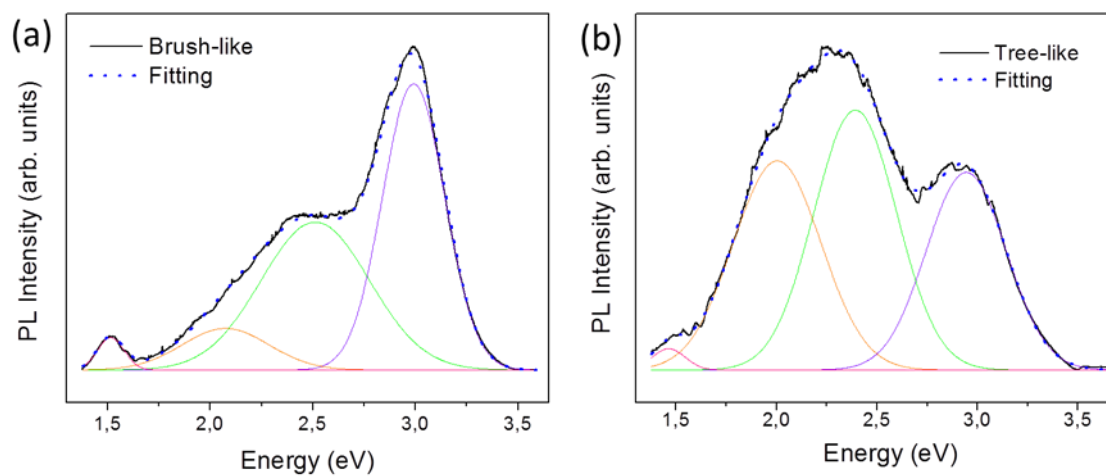
Figure S1. Raman spectrum acquired on the pellet surface of the S-800 sample.

Figure S2. (a) ESD spectrum acquired in the nanostructures of the S-800 sample. (b) SEM image of a brush-like nanostructure and (c, d) the corresponding compositional mapping of O and Sn, respectively.

Figure S3. Deconvolution of the CL spectrum obtained in the S-800 sample.

Figure S4. Deconvolution of the PL spectra acquired in the (a) brush-like and (b) tree-like samples.

M. García-Tecedor (http://www.inam.uji.es/users/miguel-garc%C3%ADa-tecedor)